RSC Advances

ROYAL SOCIETY OF CHEMISTRY

www.rsc.org/advances

Facile preparation of carbon-functionalized ordered magnetic mesoporous silica composites for highly selective enrichment of N-glycans†

Quanqing Zhang, [ab] *Qinghe Zhang,* [*a] *Zhichao Xiong,* [b] *Hao Wan,* [b] *Xiaoting Chen,* [a] *and Hanfa Zou* [b]

ABSTRACT:

Highly selective and efficient enrichment of glycans from complex biological samples is of great significance for the discovery and diagnosis of disease via identifying the related biomarkers. Mesoporous carbon materials were widely employed for the selective enrichment of glycans since the strong interactions between carbon and glycans. In this study, a novel carbon-functionalized ordered magnetic mesoporous silica composites (denoted as Fe_3O_4@3SiO_2@mSiO_2-C) with a core-shell structure, high carbon content, excellent hydrophilic property and unique magnetic character was designed and synthesized. A tactful strategy involving CTAB as the mesoporous structure-directing agent and the carbon precursor during the in-situ carbonization

[a] *Division of Metrology in Chemistry, National Institute of Metrology, Beijing 100029, China. E-mail: qhzhang204@163.com Tel:86-010-64524783.*

[b] *CAS Key Laboratory of Separation Sciences for Analytical Chemistry, National Chromatographic R&A Center, Dalian Institute of Chemical Physics, Chinese Academy of Sciences (CAS), Dalian 116023, China. E-mail: hanfazou@dicp.ac.cn. Tel: 86-411-84379610.*

were proposed. Besides, a compact silica layer with adequate thickness was essential to protecting the magnetic core during the sulphonation process in further high-temperature calcination. As a result, the obtained Fe_3O_4@3SiO_2@mSiO_2-C composites exhibited a high carbon content (25 %) with graphite structure, rapid magnetic separation (within 10 s), large pore volume (0.257 m^3 g^{-1}), high BET surface area (269.14 m^2 g^{-1}) and the well-ordered mesostructure (3.39 nm). In addition, a strong magnetic response with a saturation magnetization value (59.8 emu g^{-1}) has been confirmed. By taking the advantage of the special interaction between the carbon and glycans, the size-exclusion ability, highly hydrophile as well as unique magnetic property, the Fe_3O_4@3SiO_2@mSiO_2-C composites exhibit satisfying enrichment ability in glycomic analysis. Better selectivity and efficiency than active carbon have been confirmed. Furthermore, 42 N-linked glycans with sufficient peak intensities were obtained from human serum after treatment with the Fe_3O_4@3SiO_2@mSiO_2-C composites, showing great potential as a tool for the enrichment and detection of glycans in biological samples.

Keywords: mesoporous carbon, magnetic nanocomposits, glycopeptides, mass spectrum

1. Introduction

Since the mesoporous silica materials was invented in the early 1990s,[1, 2] mesoporous materials were confirmed to have well-defined mesoporous structure, large surface area and narrow pore size distribution, as a result, it has been widely concerned in the fields of adsorbent, sensor, catalyst, and nanodevice.[3–7] Enormous research enthusiasm have been triggered by carbon materials with regular mesoporous systems.[8–10] Due to the fascinating characteristics such as tunable pore size and mesostructure, exceptional thermal and chemical stability and strong hydrophobicity, great potential has been processed in variety applications such as drug delivery, energy storage and conversion, adsorption and separation.[11–13] It is particularly attractive to explore the approach to enhance and/or extend the properties of mesoporous carbon materials by forming nanocomposites. Therefore, various targeted applications has been designed based on cooperative and synergic effects between the mesostructure carbon and other active nanoparticles.[14]

In recent years, magnetic separation has become an ideal separation technique by taking advantage of the strong magnetic response.[15, 16] Functionalized magnetic materials with desirable building blocks or components have been popularly used in the proteomic research.[17, 18] Combining the superior properties of mesoporous carbon and the rapid magnetic responsivity of magnetic materials to build magnetic

mesoporous carbon composits is a promising way for better separation and enrichment. [19, 14]

Several methods have been taken to synthesize magnetic mesostructure carbon materials, such as thermal treatment of organometallic compounds, silica template etching processes and co-casting methods. [1, 2, 6, 8, 20–23] For the thermal treatment of organometallic compounds method, it is feasible for majority of the metal catalysis, but the morphology and metal size are difficult to control. Meanwhile, most of the materials synthesized by this method are lack of magnetic response.[24] The method of etching silica template can solve the problems above, but the etching processes may weaken the mechanical strength. Moreover, the introduction of carbon precursor involved multiple steps which are time-consuming and difficult to manipulate. The co-casting method also faced with the problem of cumbersome and weak magnetic response. As a result, the design and synthesis of magnetic mesoporous carbon materials with facile, stable and convenience process is still attracting attention. Nevertheless, the complicated and time-consuming multistep procedure to obtain these materials is an ineluctable drawback to an extensive use.[25] Therefore, it was highly desired for a simpler approach to prepare ordered mesoporous carbon materials.[26, 27]

Glycosylation is a ubiquitous and essential protein post-translation modification which attribute to the involvement in a mass of pathological and physiological process such as cell adhesion, cell growth and cell-cell recognition, etc.[28, 29] Mass spectrometry is widely used in glycan profiling for glycosylation research. However, due to the interference of proteins and the low concentration of glycans, the glycan signals from complex biological samples are usually unacceptable. Therefore, it is of great significance developing enrichment material for selective isolation of glycans digested from proteins.[30–32] Several mediums for selective enrichment of glycans have been reported. For instance, active carbon material is a promising medium based on the hydrophobic and polar interactions between carbon and glycans, however, complex proteins still been adsorbed due to the weak size-exclusion ability.[33–35] Thus functionalized mesoporous carbon materials triggered great interesting for selective enrichment of glycans.

Herein, a kind of magnetic core-shell composite with a carbon-functionalized mesoporous silica shell were synthesized using a system combined surfactant-template involved one-pot sol-gel method with the in-situ carbonization strategy. A compact silica layer was introduced to protect the magnetic core during the sulfuric acid pretreatment which was indispensable for the further carbonization. Then a mesoporous shell was directly coated on the silica layer. The structure-directing agent

CTAB was in-situ carbonized on the inner surface of the mesoporous framework forming a graphitized carbon film. The as prepared composites possessed several considerible merits for glycan enrichment, such as the well-ordered mesostructure with suitable pore size, high content of graphited carbon which can enrich glycan by polar interactions and strong hydrophilic,[36] the high BET surface area can enhance the enrich efficiency and the excellent magnetic responses helps to achieve better isolation efficiency. By taking advantage of these characteristics, the novel composites were employed to enrich N-linked glycans from human serum samples with high efficiency and selectivity.

2. Experimental details

2.1. Reagents and materials

Tetraethyl orthosilicate (TEOS, 99%), cetyltrimethyl ammonium bromide (CTAB), sulfuric acid (98%), sinapinic acid (SA), ammonium solution (25 wt%), 2,5-dihydroxybenzoic acid (2,5-DHB), and bovine serum albumin (BSA), Standard glycoprotein (chicken ovalbumin) were purchased from Sigma (St. Louis, MO, USA). Urea, dithiothreitol (DTT) and iodoacetamide (IAA) were obtained from BioRad (Hercules, CA, USA). PNGase F was acquired from New England Biolab (Ipswich, MA). Ultrafiltration membrane with MWCO of 10 KDa was acquired from Millipore

(Bedford, MA). Human serum from healthy volunteers was provided by Dalian Medical University and stored at -80 ℃ before analysis. Acetonitrile (ACN) was purchased from Merck (Darmstadt, Germany). Deionized water used for all experiments was purified with a Milli-Q water system. All other chemicals were of analytical grade and purchased from Aladdin Corporation (Shanghai, China).

2.2. Apparatus and measurements

Transmission electron microscopy (TEM) was conducted on a JEOL 2000 EX electronic microscope with an accelerating voltage of 120 keV. Fourier transform infrared (FT-IR) spectroscopy characterization was conducted on a Thermo Nicolet 380 spectrometer using KBr pellets (Nicolet, Wisconsin, USA). The nitrogen adsorption-desorption measurement of Fe_3O_4@nSiO_2@mSiO_2-C was conducted at -196 ℃ (liquid nitrogen temperature) using a static-volumetric method on an ASAP 2010 (Micromeritics, USA). The pore diameter and distribution curves were calculated by the Barrett-Joyner-Halenda (BJH) method from the adsorption branch. The saturation magnetization curve was obtained at room temperature on a Physical Property Measurement System 9T (Quantum Design, San Diego, USA). The Raman spectra were obtained on a Via-Reflex with excitation from an argon ion laser (532 nm). Thermogravimetric analysis (TGA) was performed on a Netzsch STA 409 PC thermal analysis system (NETZSCH, Selb, Germany) under air flow. All MALDI-

TOF-MS analysis results were achieved using an UltrafleXtreme MALDI-TOF/TOF System (Bruker Daltonics, German) equipped with a 1 kHz OptiBeamTM on-axis laser.

2.3. Preparation of compact silica layer coated magnetic composite

Firstly, magnetic composites were synthesized according to the method reported previously.[37] 200 mg of the prepared magnetic nanoparticles were dispersed in the solvents (160 mL ethanol, 40 mL deionized water, and 2 mL 25% ammonia solution) and sonicated for 0.5 h. Next, 1.5 mL TEOS was added into the flask drop by drop, and the mixture was mechanically stirred at room temperature for an additional 12 h. The above process was repeated for three times to form a dense and thick shell encapsulating the magnetic core. Then the obtained material was washed with deionized water and ethanol for three times by magnetic separation and dried under vacuum at 60 ℃ for the next step of the experiment.

2.4. Synthesis of ordered mesoporous silica coated magnetic composite

According to the reported methods by Deng's group.[38, 39] By using the obtained acidulated Fe_3O_4@nSiO_2 composites as supporter, a mesoporous silica layer was coated on the surface of Fe_3O_4@nSiO_2 composites through a surfactant-template involved one-pot sol-gel method. First of all, 57 mg acidulated Fe_3O_4@nSiO_2 composites and 370 mg CTAB were dispersed in the solvent (56 mL ethanol, 94 mL

deionized water, and 1.2 mL 25% ammonia solution) and then mechanically stirred for 0.5 h in a three-necked bottle. Secondly, 800 μL TEOS was added into the stabilized dispersion-solution dropwise and went on mechanically stirring for more 20 h at room temperature. Then the obtained material (Fe_3O_4@nSiO_2@mSiO_2-CTAB) was washed with deionized water and ethanol for three times by magnetic separation and dried under vacuum at 60 ℃ overnight.

Afterwards, 50 mg obtained Fe_3O_4@nSiO_2@mSiO_2-CTAB composites and 500 mg $(NH_4)_3NO_3$ was dispersed in 50 mL ethanol, and then the mixture was mechanically stirred for 24 h at room temperature to wipe out CTAB. The obtained Fe_3O_4@nSiO_2@mSiO_2 composites was washed with deionized water and ethanol for three times by magnetic separation and dried under vacuum at 60 ℃.

2.5. Synthesis of carbon-functionalized ordered mesoporous silica coated magnetic composite

The as-prepared Fe_3O_4@nSiO_2@mSiO_2-CTAB composites were dispersed in an acidic solution including 12 mL of deionized water and 500 μL of concentrated sulfuric acid (98 wt%), followed by mechanical stirring at room temperature for 30 min. Then the mixed solution was heat-treated at 100 ℃ for 12 h, afterwards, the temperature was transfered to 160 ℃ for additional 12 h heat-treat under air atmosphere. In the end, the sulfuric acid pretreated compound was calcined at 300 ℃

(3 ℃ min^{-1}) for 3 h and then 700 ℃ (3 ℃ min^{-1}) for 3 h under nitrogen atmosphere to obtain the ultimate product.

2.6. Preparation of protein digests

1 mg of chicken ovalbumin (OVA) was dispersed in 1 mL 25 mM ammonium bicarbonate buffer at pH 7.5. Then the mixed solution was boiled for 6 minutes make the protein degeneration. Afterwards, the PNGase F (10 U) was added into 100 μL the mixed solution which has been denatured and then incubated at 37 ℃ for 24 h.

Before zymolytic, human serum was centrifuged at 12000 r for 10 min. The obtained supernatant (50 μL) was mixed with ammonium bicarbonate (25 mM, pH 7.5, 450 μL) and denatured in a boiling water bath for 5 min. Then ultrafiltration membrane was used to filter out the endogenous peptides at 12000 r for 20 min. The obtained deposition was washed by ammonium bicarbonate (200 μL) for three times, and dissolved in ammonium bicarbonate (25 mM, pH 7.5, 500 μL). The zymolytic process of human serum is the same as OVA.

2.7. Selective enrichment of glycans from biological samples

Fe_3O_4@nSiO_2@mSiO_2-C composites (10 mg mL^{-1}, 80 μL) were added into 20 μL digests solution (ovalbumin or human serum), then adding a specified volume of deionized water to make 200 μL of total volume, incubated for 60 min. Remove the supernatant by magnetic separation and the deposition was washed with deionized

water (100 μl) for three times. At last, 20 μL 80% ACN was selected as eluent for MS analysis. As a comparison, the Fe_3O_4@nSiO_2@mSiO_2 composites and active carbon materials were studied under the same condition.

2.8. Mass spectrometric analysis

DHB (10 mg mL^{-1} 2, 5-DHB, 50% ACN-H_2O, 10 mM NaCl) was used as the matrix for the analysis of glycans. Sinapinic acid (saturated in 50% ACN-H_2O solution containing 0.1% FA) was used for the analysis of proteins. Sample aliquots (0.5 μL) were first placed on a plate, and then desiccated at room temperature, and the SA matrix (0.5 μL) was then added prior to MALDI-TOF-MS analysis.

3. Results and discussion

The Fe_3O_4@nSiO_2@mSiO_2-C composites were obtained using a system combined surfactant-template involved one-pot sol-gel method with the in-situ carbonization strategy. The detailed synthetic approach for the fabrication of Fe_3O_4@nSiO_2@mSiO_2-C composites is shown in Scheme 1. Typically, in order to acquire the non-porous silica layers coated Fe_3O_4 composites (denoted as Fe_3O_4@nSiO_2), the as-prepared mono-disperse magnetic Fe_3O_4 nanoparticles were treated with a Stöber procedure.[40] The outer mesoporous silica framework was synthesized by a sol-gel method with TEOS as the silicon precursor, and CTAB as the structure-directing agent. After that, a carbon film was directly in-situ carbonized on

the inner surface of the mesoporous silica framework with CTAB as the carbon precursor.[41] Importantly, the carbonization rate of CTAB might decrease since it is possible to degrade under high temperature, so the pretreatment of Fe_3O_4@3SiO_2@mSiO_2−CTAB composites before calcination is necessary.[40, 42–43] In this work, a pretreatment of H_2SO_4 at a lower temperature before carbonization was taken to improve the carbonization rate of CTAB. Compared with the conventional syntheses of mesoporous carbon materials, the novel method simplified the structure-directing agent removal and the carbon source addition processes which were time-consuming, difficult to operate and risky to collapse the structure.

<Scheme 1>

Since the sulfuric acid pretreatment is likely to destroy the magnetic core due to the strong corrosivity. So it is worth to mention that the formation of the compact silica was the critical step in the preparation of core-shell structure. As shown in Fig. 1, materials coated with compact silica layers 1, 2 or 3 times corresponding to the thickness of 15 nm, 25 nm, 45 nm (roughly estimated by TEM images) was assembled separately. It was found that the material with the silica layer thickness of only 15 nm spoiled extremely serious while treated with sulfuric acid. And the material with silica layer thickness of 25 nm thick silica layer spoiled at a smaller extent while treated with sulfuric acid directly, but almost completely corroded after

coated the mesoporous shell and pretreated with sulfuric acid before carbonization. Encouragingly, the composite with the silica layer thickness of 45 nm was seldom spoiled after the whole sulphonation processes. It could be speculated that during the sulphonation process, accompany with the water evaporated at the high temperature, the concentration of H_2SO_4 solution got higher and higher. As a result, the condensed ionized H^+ from H_2SO_4 and the active mobility of H_2SO_4 solution might lead the magnetic core destruction. In this case, since the reaction between H_2SO_4 and the magnetic core impeded by the silica layer with proper thickness, the magnetic core could remain protected and the C_{16}-alky chain sulphonated more completely.

<Fig. 1>

In order to evaluate the surplus saturation magnetization values of the magnetic material in each operation, the room-temperature magnetization curve of the material was recorded as Fig. 2. Magnetic measurement shows that the magnetization values of Fe_3O_4, Fe_3O_4@3SiO_2@mSiO_2-C and Fe_3O_4@1SiO_2@mSiO_2-C are 80.1, 59.8 and 13.8 emu g^{-1}, respectively. The magnetization value of the material coated with compact silica layer only 1 time is much weaker than that of the pure magnetic core. The result further indicates that the compact layer with too thin thickness failed to protect the magnetic core. In striking contrast, after sulfonation treatment, the as-prepared Fe_3O_4@3SiO_2@mSiO_2-C composites still show strong magnetization value

which is extremely close to the magnetization value of pure magnetic core. And this property suggesting a good suitability for magnetic separation.[36] The desirable performance benefits from the compact silica layer with an appropriate thickness which protected the magnetic core from the etch of H_2SO_4, meanwhile, the thickness of the layer is not too thick to interference the magnetization responses. In addition, the in-situ carbonization method retained the silica template, and this strategy avoided the template remove process which may impact the structure and magnetic responses of the composites.

<Fig. 2>

Fe_3O_4@3SiO_2@mSiO_2-C still shows an excellent dispersibility in aqueous solution (Fig. 3) despite a hydrophobic carbon film was coated on the inner surface of the mesoporous. That benefit from the hydrophilic groups exposed on the surface of silica framework which was completely retained during the whole synthetic progress, and there are abuntant hydrophilic hydroxyl groups exposed on it either. Conventional mesoporous carbon materials is poorly soluble in aqueous solution,[44] which might result in serious agglomeration, slow interaction, and severe aggregation and adhesion on the tube. The excellent dispersibility in aqueous solution of Fe_3O_4@3SiO_2@mSiO_2-C can efficiently eliminate the defects so that the application fields enlarged.

<Fig. 3>

Compared with carbon-based mesopours materials, silica-based mesoporous materials have much better mechanical strength. That may have some adverse effects during the separation processes, such as ultrasonic treatment, mechanical stirring. The retaining silica framework can efficiently enhance the mechanical strength of the material which is crucial for the application under high pressure or high strength.

To elucidate the form of interstitial structure in the Fe_3O_4@3SiO_2@mSiO_2-C, the nitrogen sorption measurements have been taken (Fig. 4). The abrupt increase of P/P_0 from 0.40 to 0.80, suggesting the well-ordered mesoporous pore size distribution. It is estimated that the Brunauer-Emmett-Teller (BET) surface area of the composites r 269.14 m^2 g^{-1}.[45] The pore diameter aperture distribution curve according to the Barrett-Joyner-Halenda (BJH) model indicates that the composites have a large pore volume of 0.257 m^3 g^{-1}. And a well-ordered mesoporous pore structure with a narrow pore-size distribution centered at 3.39 nm was confirmed.

<Fig. 4>

The carbon content and the morphology of carbon have been investigated by TGA, FT-IR spectra and Raman spectra. The TGA and DTG curves of Fe_3O_4@3SiO_2@mSiO_2 and Fe_3O_4@3SiO_2@mSiO_2-C had shown in Fig. 5. The maximum weight loss of Fe_3O_4@3SiO_2@mSiO_2-C (about 25%) can be observed

between 400 and 500 ℃. It indicates that the carbon content of Fe_3O_4@3SiO_2@mSiO_2-C reached 25 %. DTG curve shows the maximum weight loss temperatures of Fe_3O_4@3SiO_2@mSiO_2 (180 ℃) and Fe_3O_4@3SiO_2@mSiO_2-C (450℃). It is interesting to find that the maximum weight loss temperature increased about 270 ℃ after in-situ carbonization, and that might be due to the existing form of carbon changed substantially.

<Fig. 5>

The FT-IR spectra of Fe_3O_4@3SiO_2@mSiO_2-CTAB and Fe_3O_4@3SiO_2@mSiO_2-C were compared in Fig. 6. The strong peaks of C-H_x (2925 cm^{-1} , 2983cm^{-1}) become much weaker after in-suit carbonization. Meanwhile, the intensity of C=C (from 1620 cm^{-1} to 1680 cm^{-1}) enhanced which means the C_{16}-alkyl chains of CTAB were transferred to an aromatic nucleus structure with π-π bonds after the pretreatment of sulphuric acid and carbonization.[46]

<Fig. 6>

As characterized by Raman spectroscopy (Fig. 7), two peaks around 1340 cm^{-1} (D-MODE) and 1580 cm^{-1} (G-MODE) were observed. The G-MODE is characteristic of alkene stretching vibrations and suggests the formation of C=C linkages because of dehydration reaction catalyzed by the sulphuric acid.[46] Simultaneously, the peak of G-MODE is much higher than that of D-MODE, further reflecting a high graphitic

crystallinity of the carbon containing in Fe_3O_4@3SiO_2@mSiO_2-C.[40] The obviously changed existing form of carbon from chain to graphitized carbon could result in highly enhanced hydrophobicity and thermostability, and that coincide with the result of thermogravimetric analysis.

<Fig. 7>

The characteristic result indicates that the well-ordered mesoporous structure has a perfect cutoff size to exclude most highly abundant proteins (such as HSA; 67 kDa, 5 nm × 7 nm × 7 nm).[47] And the high content of graphitized carbon signifying considerable efficiency in the enrichment of glycans by the hydrophobic and polar interactions between carbon and glycans.[33, 34] So it is of great potential to selective enrich the glycans and efficiently size-exclude the highly abundant large proteins in biological fluids digests.

On the basis of the high carbon content, the outstanding dispersibility in aqueous solution, the strong magnetic response and the well-ordered mesoporous structure, Fe_3O_4@3SiO_2@mSiO_2-C was adopted for the development of an effective separation and enrichment approach, aiming at enriching the low abundance, low molecule wright N-linked glycans in protein digests and human serum. The polor interactions between carbon and glycans, size exclusion of high molecular weight proteins by the

mesoporous, and the rapid separation of magnetic microsphere would be conducive to enhancing the enrichment efficiency.[36]

In order to inspect the feasibility of N-linked glycan enrichment, the Fe_3O_4@3SiO_2@mSiO_2-C composites were applied to enrich the N-linked glycans in the ovalbumin digests (Fig. 8). Fig. 8a shows that a few N-linked glycan was detected with low intensities and signal to noise ratio before enrichment. After the enrichment with Fe_3O_4@3SiO_2@mSiO_2-C (Fig. 8c), no N-linked glycans can be detected. And no protein signal in the elution after enriched by Fe_3O_4@3SiO_2@mSiO_2-C (Fig. 8b). Compared with the protein detection before enrichment (Fig. 8d), the signal intensity declined obviously. The above results suggest that Fe_3O_4@3SiO_2@mSiO_2-C composites are possible medium to selective enrichment the N-linked glycans with excellent size- exclusion.

<Fig. 8>

The highly enrichment selectivity of Fe_3O_4@3SiO_2@mSiO_2-C was evaluated by using a more complex sample containing a certain amount of ovalbumin digests with different amount of BSA as the interfere protein (Fig. 9). As shown in Fig. 9a, after enriched by Fe_3O_4@3SiO_2@mSiO_2-C, there were 25 N-linked glycans detected with high signal intensities when the ratio of BSA to OVA was 0:1. After the extraction with active carbon (Fig. 9b), a total of 24 N-linked glycans were detected. The highest

intensity of glycans enriched by Fe_3O_4@3SiO_2@mSiO_2-C reached 12000, as much as twice of that enriched by active carbon. When the ratio increased to 10:1, only a few signal intensity decreased, and there are still 25 N-linked glycans can be detected after enriched by Fe_3O_4@3SiO_2@mSiO_2-C (Fig. 9c). In comparison, after being enriched by active carbon (Fig. 9d), only 21 N-linked glycans signal observed in the MS spectrum (S/N >3), and that might be due to the interference of protein. After enrichment with Fe_3O_4@3SiO_2@mSiO_2-C, there are still strong signal intensities of 25 N-linked glycans detected even though the ratio of BSA to ovalbumin increased to 50:1 (Fig. 9e). Activated carbon was also used for comparison (Fig. 9f), the signal intensity of N-linked glycans decreased obviously, and only 19 N-linked glycans can be detected. The highest intensity of glycans enriched by Fe_3O_4@3SiO_2@mSiO_2-C is 7000, and there are only less than 1200 of that enriched by active carbon. As Fig. S1† shows, after enriched with active carbon, there are still proteins detected in the eluant which means the size-selectivity of active carbon is not enough. Briefly, compared with active carbon materials, the intensity of N-linked glycans enriched by Fe_3O_4@3SiO_2@mSiO_2-C composites are much stronger, and since the content of interfering proteins increased, the more obvious superior size-exclusion shows. This result illustrates that the Fe_3O_4@3SiO_2@mSiO_2-C composites have outstanding size-exclusion performance in eliminating the interference of large-size proteins, which

indispensable for glycans profiling and indicating the better size selectivity of proteins.

<Fig. 9>

There are close connections between glycan in human serum and many diseases;[48] therefore, the research to selective enrich glycans in human serum for further analysis is of great scientific significance. As shown in Fig. S2†, there almost none glycans can be detected before enrichmen. Encouragingly, after the enrichment with Fe_3O_4@3SiO_2@mSiO_2-C composites, 41 N-linked glycans with obviously stronger signal intensities were detected (Fig. 10) in 200 μL human serum. The detail structure of detected N-linked glycans was displayed in Table S1†. To evaluate the reusability of Fe_3O_4@3SiO_2@mSiO_2-C composites, the used material was reused to enrich the glycans from human serum in the same way, and two groups were treated at the same time to evaluate the stability. As shown in Fig. S3†, the stability and reusability is excellent, the highest intensity are very close ($4x10^4$) and also 41 glycans can be detected. All the results above suggest that the Fe_3O_4@3SiO_2@mSiO_2-C composites have excellent performance in N-linked glycans enrichment from complex bio-samples.

<Fig. 10>

4. Conclusions

In summary, carbon-functionalized ordered magnetic mesoporous silica composites with core-shell structure have been successful prepared by surfactant-template involved one-pot sol-gel method combined with a facile in-situ carbonization strategy. A precisely controlled non-porous silica layer was coated previously to protect the magnetic core from being spoiled by H_2SO_4 and help to establish the outer mesoporous shell. A large pore volume (0.257 m^3 g^{-1}), high BET surface area (269.14 m^2 g^{-1}) and the well-ordered mesostructure with a narrow pore-size distribution centered at 3.39 nm could be obtained. Moreover, a strong magnetic response with a saturation magnetization value of 59.8 emu g^{-1} has been confirmed. The content of highly graphitized carbon structure reached 25% which is indispensible for glycan enrichment. Using the novel materials, 41 N-linked glycans from human serum were enriched with excellent selectivity and efficiency, also outstanding size-exclusion has been confirmed. It can be concluded that the obtained Fe_3O_4@3SiO_2@mSiO_2-C composites have great potential in the application of glycomics research.

Acknowledgements

The authors acknowledge funding support from the Scientific Instruments Special Projects (2012YQ09016703), the China State Key Basic Research Program Grant (2013CB-911203, 2012CB910601), the Creative Research Group Project of NSFC

(21321064), and the Knowledge Innovation program of DICP to Hanfa Zou as well as the National Natural Sciences Foundation of China (No. 21175133, 21235006)

Notes and references

1. J. S. Beck, J. C. Vartuli, W. J. Roth, M. E. Leonowicz, C. T. Kresge, K. D. Schmitt, C. T. W. Chu, D. H. Olson, E. W. Sheppard, S. B. Mccullen, J. B. Higgins and J. L. Schlenker, *J. Am. Chem. Soc*., 1992, **114**, 10834.
2. T. Yanagisawa, T. Shimizu, K. Kuroda and C. Kato, *Bull. Chem. Soc. Jpn*., 1990, **63**, 988.
3. G. Yao, D. Qi, C. Deng and X. Zhang, *J. Chromatogr. A*, 2008, **1215**, 82–91.
4. S. H. Joo, S. J. Choi, I. Oh, J. Kwak, Z. Liu, O. Terasaki and R. Ryoo, *Nature*, 2001, **414**, 470.
5. P. Yang, T. Deng, D. Zhao, P. Feng, D. Pine, B. F. Chmelka, G. M. Whitesides and G. D. Stucky, *Science*, 1998, **282**, 2244.
6. C. Liang, Z. Li and S. Dai, *Angew. Chem., Int. Ed*., 2008, **47**, 3696.
7. A. Vinu, C. Streb, V. Murugesan and M. J. Hartmann, *Phys. Chem. B*, 2003, **107**, 8297.
8. R. Ryoo, S. H. Joo and S. J. Jun, *Phys. Chem. B*., 1999, **103**, 7743.
9. Y. Meng, D. Gu, F. Zhang, Y. Shi, H. Yang, Z. Li, C. Yu, B. Tu and D. Zhao, *Angew. Chem. Int. Ed*., 2005, **117**, 7215.
10. Y. Meng, D. Gu, F. Zhang, Y. Shi, L. Cheng, D. Feng, Z. Wu, Z. Chen, Y. Wan, A. Stein and D. Zhao, *Chem. Mater*., 2006, **18**, 4447.
11. Z. Wu and D. Zhao, *Chem. Commun*., 2011, **47**, 3332.
12. H. Zhou, S. Zhu, M. Hibino, I. Honma and M. Ichihara, *Adv. Mater*., 2003, **15**, 2107.

13. H. Wan, H. Qin, Z. Xiong, W. Zhang and H. Zou, *Nanoscale*, 2014, **6**, 8743.
14. Z. Wu, W. Li, P. A. Webley and D. Zhao, *Adv. Mater*., 2012, **24**, 485.
15. W. Ma, L. Li, Y. Zhang, Q. An, L. You, J. Li, Y. Zhang, S. Xu, M. Yu, J. Guo, H. Lu and C. Wang, *J. Mater. Chem*., 2012, **22**, 23981.
16. Z. Feng, S. Zhu, D. R. Martins de Godoi, A. C. Samia and D. Scherson, *Anal. Chem*., 2012, **84**, 3764.
17. Z. Xiong, L. Zhang, C. Fang, Q. Zhang, Y. Ji, Z. Zhang, W. Zhang and H. Zou, *J. Mater. Chem. B*, 2014, 2, 4473.
18. Z. Xiong, Y. Ji , C. Fang, Q. Zhang, L. Zhang, M. Ye, W. Zhang and H. Zou, *Chem. Eur. J.*, 2014, 20, 7389.
19. J. Liu, S. Qiao, Q. Hu and G. Lu, *Small*, 2011, **7**, 425.
20. T. Muraliganth, A.V. Murugan and A. Manthiram, *Chem. Commun*., 2009, **45**, 7360.
21. X. Dong, H. Chen, W. Zhao, X. Li and J. Shi, *Chem. Mater*., 2007, **19**, 3484.
22. C. Wang, J. Wang and Z. Sheng, *J. Phys. Chem*., 2007, **111**, 6303.
23. Q. Zhu, Q. Pan and F. Liu, *J. Phys. Chem*., C. 2011, **115**, 17464.
24. J. Lee, S. Y. Lee, S. H. Park, H. S. Lee, J. H. Lee, B. Y. Jeong, S. E. Park and J. H. Chang, *J. Mater. Chem. B*., 2013, 1, 610.
25. M. Florent, C. Xue, D. Zhao and D. Goldfarb, *Chem. Mater*., 2012, **24**, 383.
26. I. Moriguchi, A. Ozono, K. Mikuriya, Y. Teraoka, S. Kagawa and M. Kodama, *Chem. Lett*., 1999, 1171.
27. Z. Li, W. Yan and S. Dai, *Carbon*, 2004, **42**, 767.
28. Y. Tian, Y. Zhou, S. Elliott, R. Aebersold and H. Zhang, *Nat. Protoc*., 2007, 2, 334.
29. A. Helenius and M. Aebi, *Science*, 2001, **291**, 2364.

30. T. M. Block, M. A. Comunale, M. Lowman and L. F. Steel, P. R. Romano, C. Fimmel, B. C. Tennant, W. T. London, A. A. Evans, B. S. Blumberg, R. A. Dwek, T. S. Mattu and A. S. Mehta, *P. Natl. Acad. Sci. USA*, 2005, **102**, 779.
31. R. Goldman, H. W. Ressom, R. S. Varghese, L. Goldman, G. Bascug, C. A. Loffredo, M. Abdel-Hamid, I. Gouda, S. Ezzat, Z. Kyselova, Y. Mechref and M. V. Novotny, *Clin. Cancer. Res*., 2009, **15**, 1808.
32. P. A. Norton, M. A. Comunale, J. Krakover, L. Rodemich, N. Pirog, A. D' Amelio, R. Philip, A. S. Mehta and T. M. Block, *J. Cell. Biochem*., 2008, **104**, 136.
33. N. H. Packer, M. A. Lawson, D. R. Jardine, J. W. Redmond, *Glycoconj. J*., 1998, **15**, 737.
34. J. Q. Fan, A. Kondo, I. Kato, Y. C. Lee, *Anal. Biochem.*, 1994, **219**, 224.
35. M. L. A. de Leoz, H. J. An, S. Kronewitter, J. Kim, S. Beecroft, R. Vinall, S. Miyamoto, R. D. White, K. S. Lam, C. Lebrilla, *Dis. Markers*, 2008, **25**, 243.
36. N. Sun, C. Deng, Y. Li, and X. Zhang, *Anal. Chem.*, 2014, **86**, 2246.
37. L. Zhao, H. Qin, Z. Hu, Y. Zhang, R. Wu and H. Zou, *Chem. Sci*., 2012, **3**, 2828.
38. P. Yin, Y. Wang, Y. Li, C. Deng, X. Zhang and P. Yang, *Proteomics*, 2012, **12**, 2784.
39. P. Yin, N. Sun, C. Deng, Y. Li, X. Zhang and P. Yang, *Proteomics*, 2013, **13**, 2243.
40. S. Gai, P. Yang, C. Li, W. Wang, Y. Dai, N. Niu and J. Lin, *Adv. Funct. Mater*., 2010, **20**, 1166.
41. P. Valle-Vigón, M. Sevilla and A. B. Fuertes, *Chem. Mater*., 2010, **22**, 2526.
42. S. Liu, H. Chen, X. Lu, C. Deng, X. Zhang, and P. Yang, *Angew. Chem*., 2010, **122**, 7719.

43. T. Ma, L. Liu and Z. Yuan, *Chem. Soc. Rev*., 2013, **42**, 3977–4003.
44. H. Qin, L. Zhao, R. Li, R. Wu, and H. Zou, *Anal. Chem.*, 2011, **83**, 7721 –7728.
45. N. Sun, X. Zhang and C. Deng, *Nanoscale*, 2015, **7**, 6487-6491.
46. G. Socrates, Infrared and Raman Characteristic Group Frequencies, 3rd ed.; Wiley: New York, 2005.
47. H. Qin, P. Gao, F. Wang, L. Zhao, J. Zhu, A. Wang, T. Zhang, R. Wu and H. Zou, *Angew. Chem. Int. Ed*., 2011, **50**, 12218.
48. K. Stumpo and V. Reinhold, *J. Proteome Res*., 2010, **9**, 4823.

Figure captions

Scheme 1 Illustration of the synthesis procedure for carbon-functionalized ordered magnetic mesoporous silica composite.

Fig. 1 TEM images of the magnetic core (a); the products coated with compact silica layer 1 (b) or 2 (c) times after sulphonation; the magnetic core coated with a 45 nm thick compact layer (d); the final obtained core-shell magnetic mesoporous carbon composites (e, f).

Fig. 2 saturation magnetization values of the pure magnetic core (a), Fe_3O_4@3SiO_2@mSiO_2-C (b) and Fe_3O_4@1SiO_2@mSiO_2-C (c).

Fig. 3 Fe_3O_4@3SiO_2@mSiO_2-C composites dispersed in water and magnetically separated.

Fig. 4 Nitrogen adsorption-desorption isotherms and pore size distribution of Fe_3O_4@3SiO_2@mSiO_2-C composites.

Fig. 5 The TGA and DTG curves of Fe_3O_4@3SiO_2@mSiO_2 (a) and Fe_3O_4@3SiO_2@mSiO_2-C (b).

Fig. 6 The FT-IR spectra of Fe_3O_4@3SiO_2@mSiO_2-CTAB (a) and Fe_3O_4@3SiO_2@mSiO_2-C (b).

Fig. 7 Raman spectrum of Fe_3O_4@3SiO_2@mSiO_2-C.

Fig. 8 MALDI-TOF MS analysis of N-glycans released from ovalbumin digests before enrichment (a) and the supernatant after (c) enrichment with Fe_3O_4@3 SiO_2@mSiO_2-C; MAL-TOF MS analysis of proteins in ovalbumin digests before enrichment (d) and the elution after (c) enrichment with Fe_3O_4@3SiO_2@mSiO_2-C.

Fig. 9 MALDI-TOF MS analysis of N-glycans released from ovalbumin digests of BSA (w/w) at 1:0, 1:10, 1:50 after enrichment with Fe_3O_4@3SiO_2@mSiO_2-C (a, c, e) and activated carbon(b, d, f). Peaks marked with are the signals of N-linked glycans.

Fig. 10 MALDI-TOF MS analysis of N-linked glycan released from human serum mixture after enriched by Fe_3O_4@3SiO_2@mSiO_2-C.

1 Scheme 1

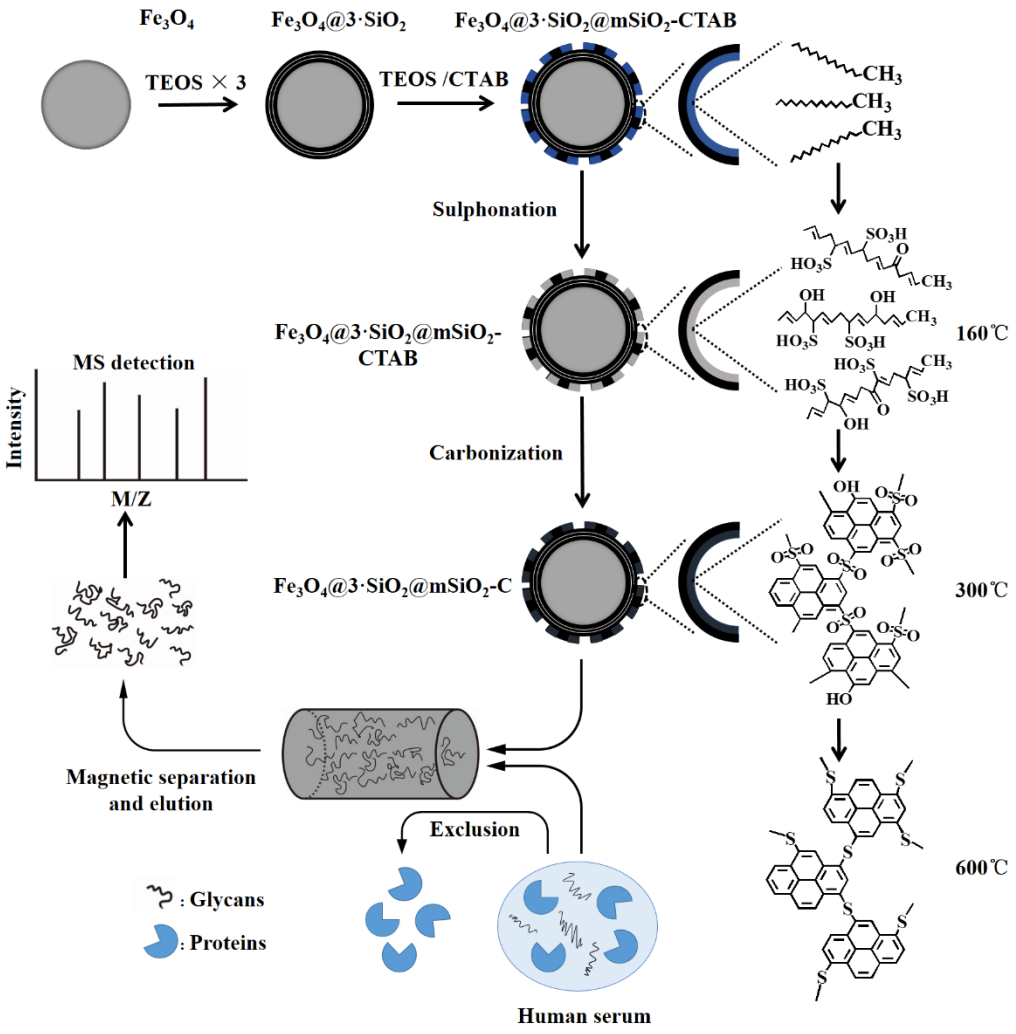

2

3

4

5

6

7

8

9

Fig. 1

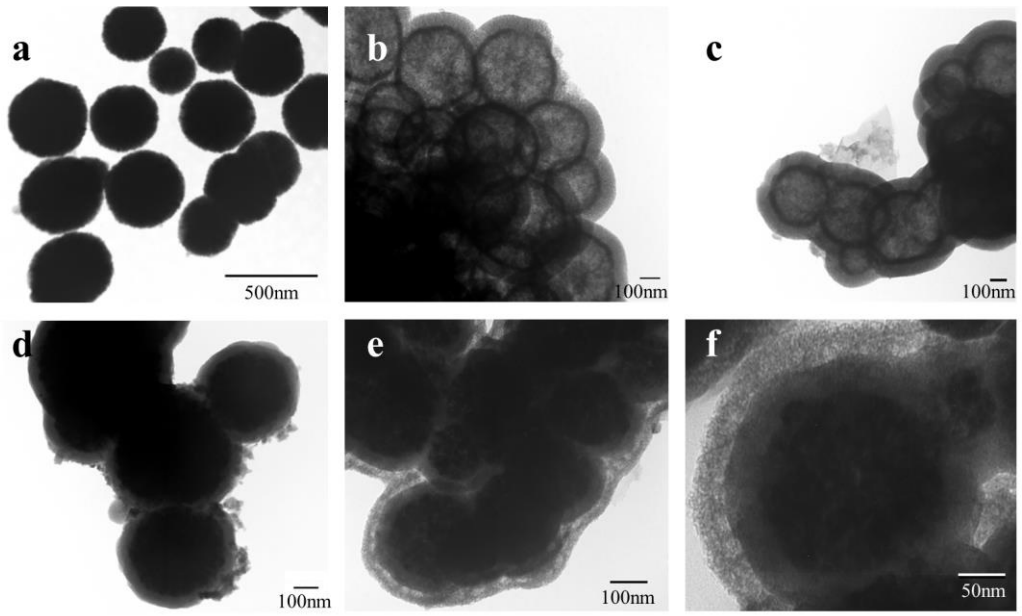

Fig. 2

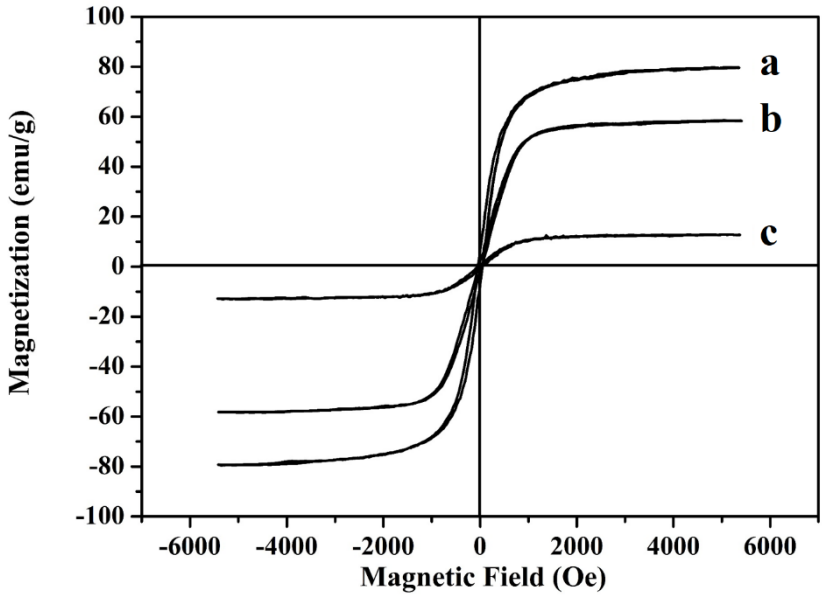

Fig. 3

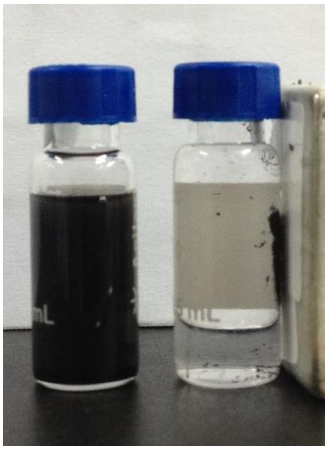

Fig. 4

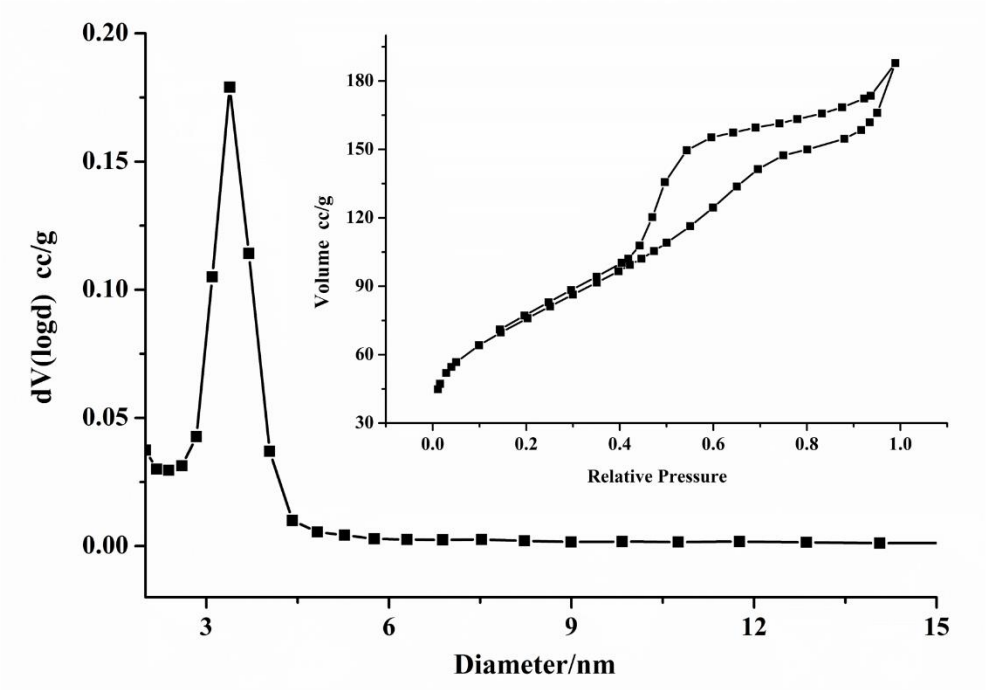

Fig. 5

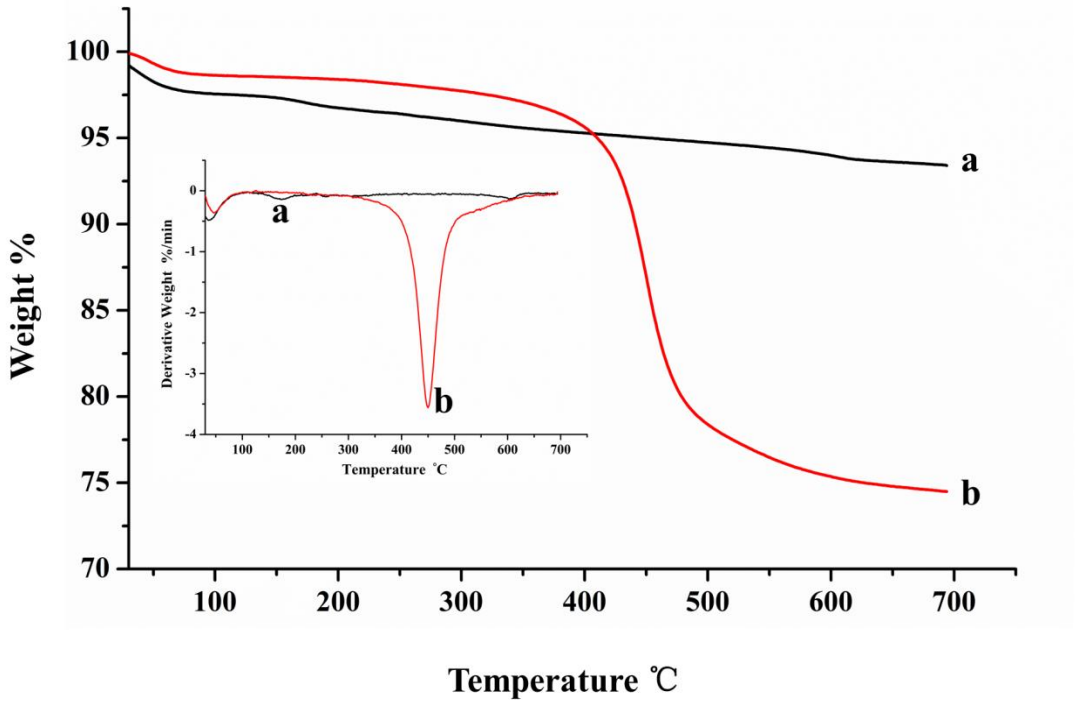

Fig. 6

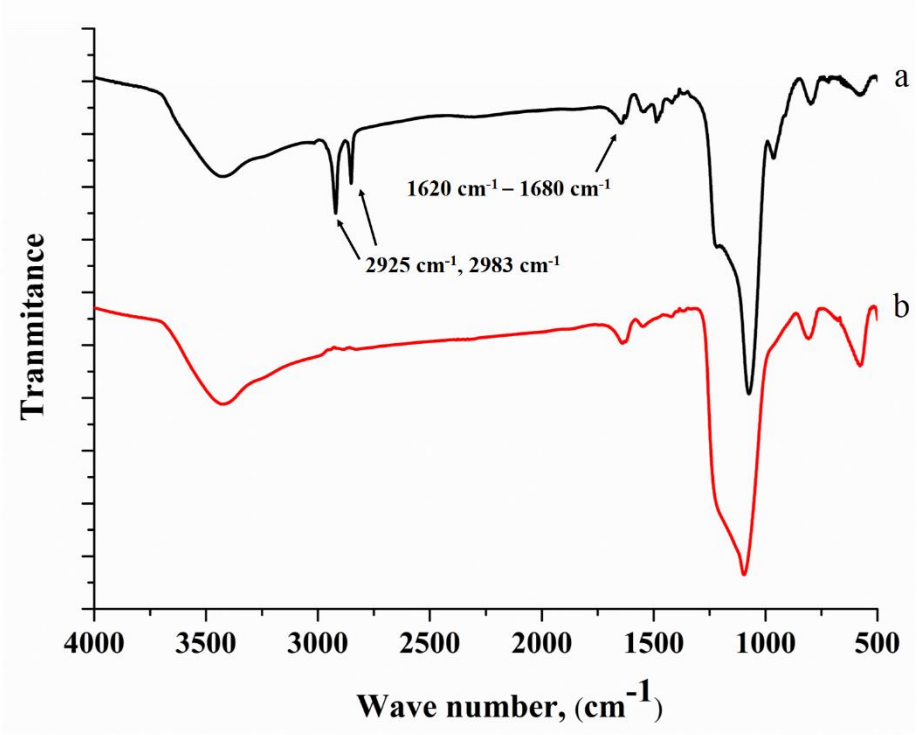

Fig. 7

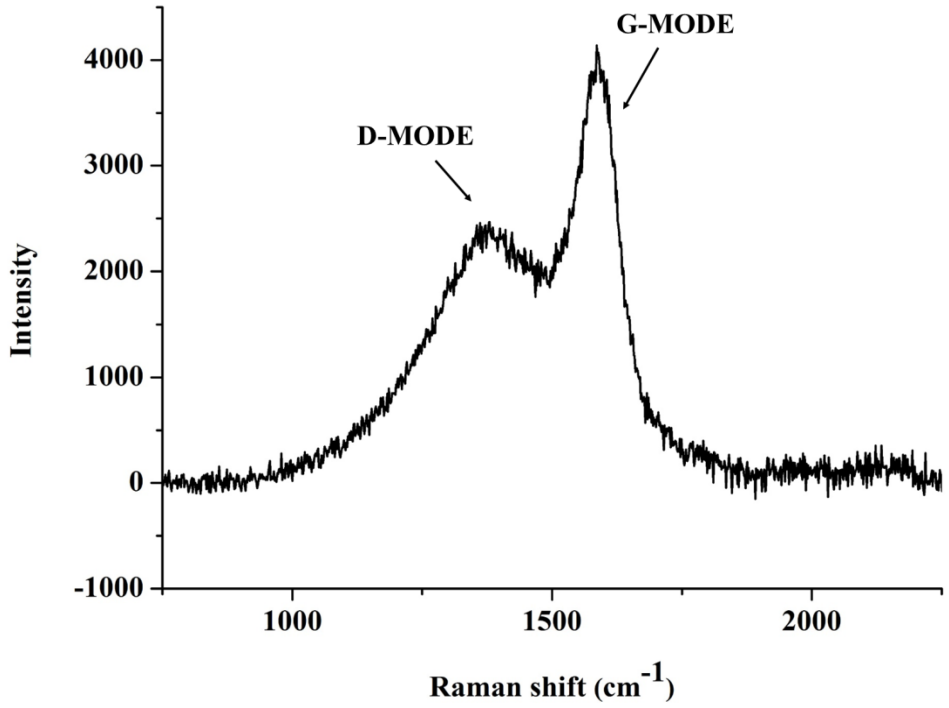

Fig. 8

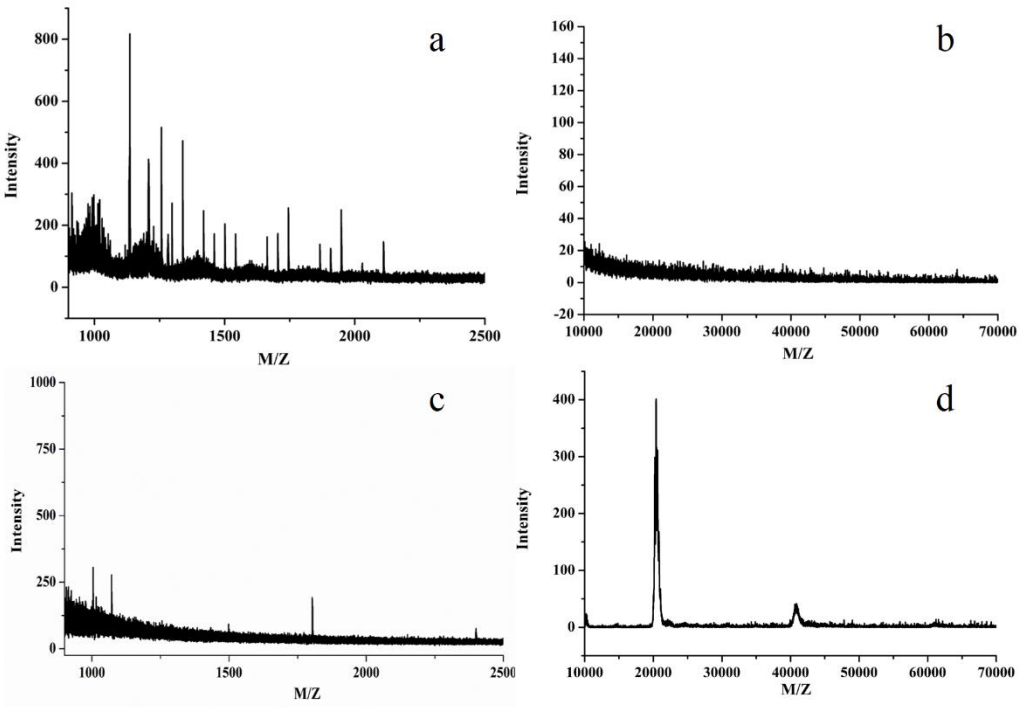

Fig. 9

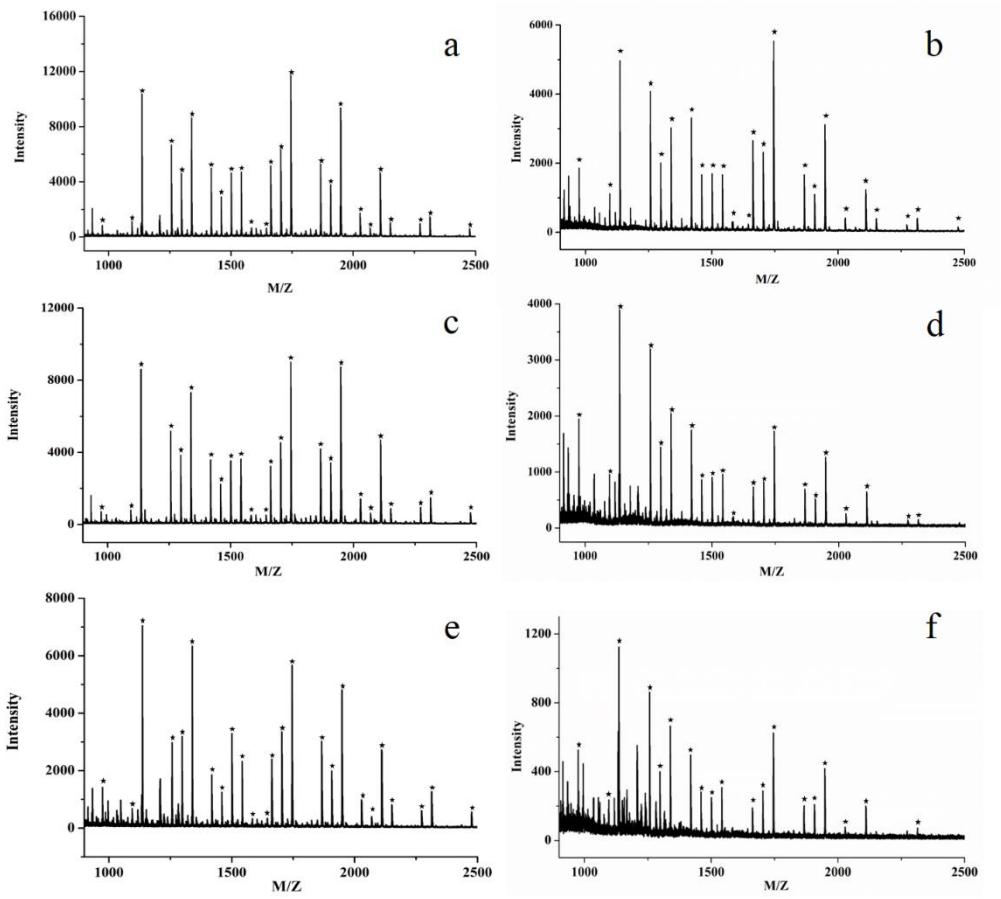

1 Fig. 10

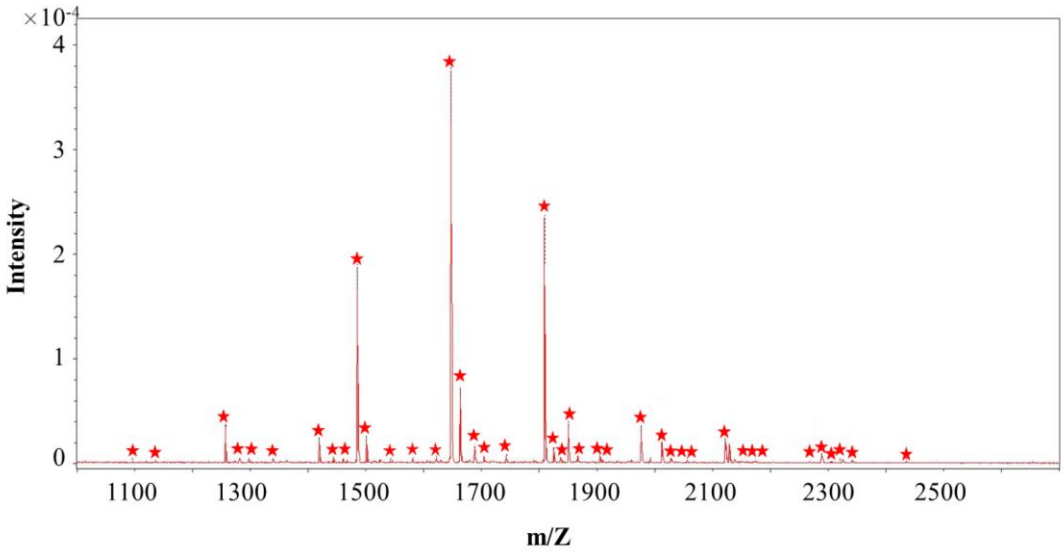

2

3

4

5

6

7

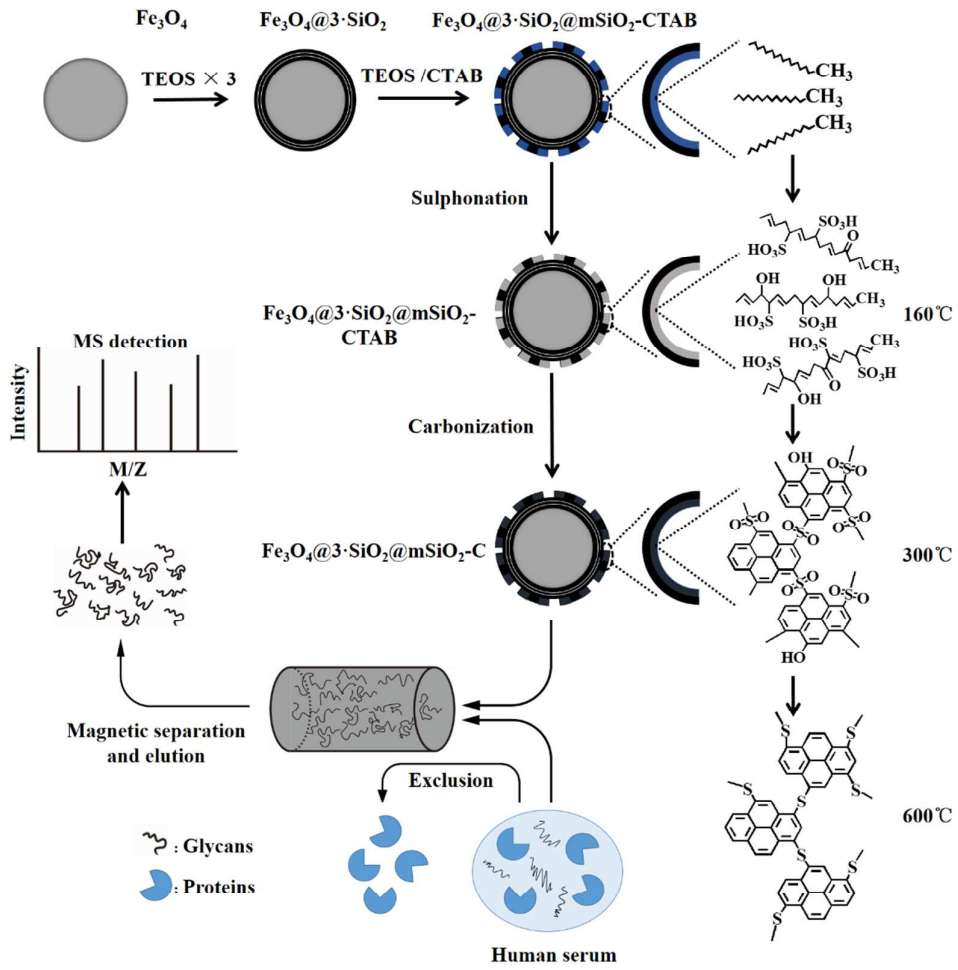

Illustration of the synthesis procedure for carbon-functionalized ordered magnetic mesoporous silica composite.

Scheme 1

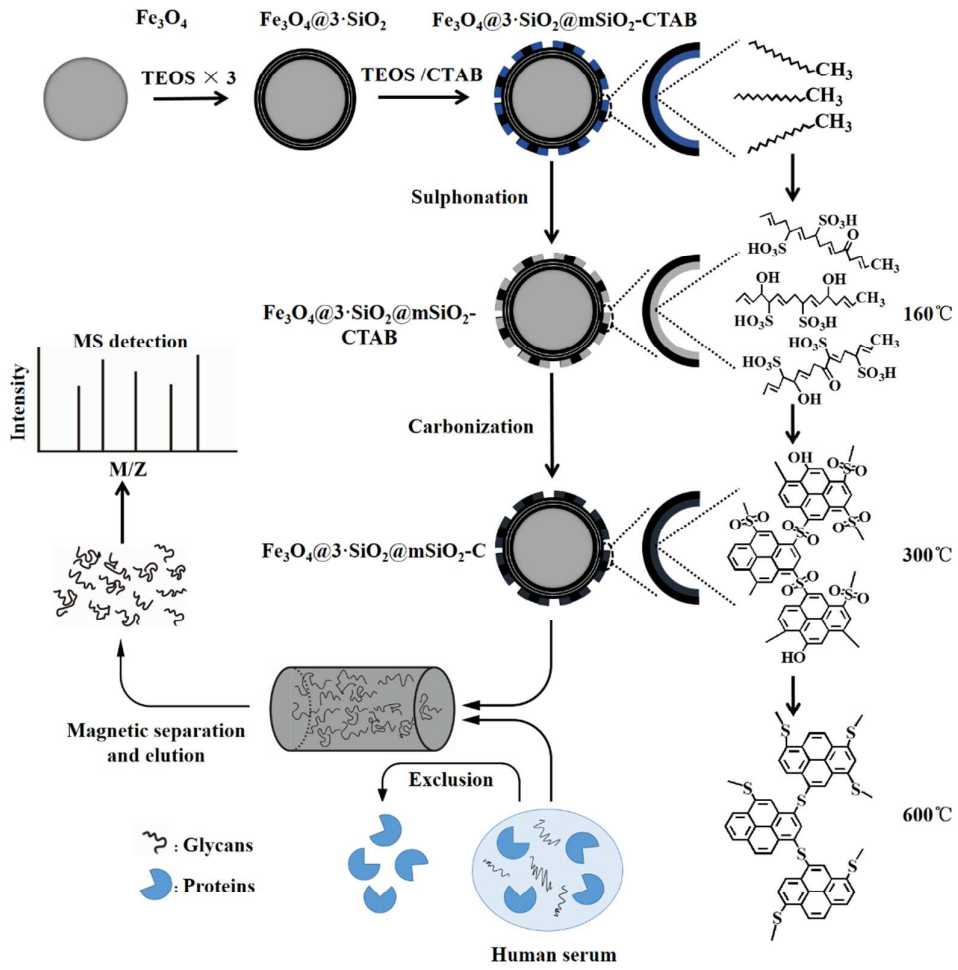

Fig. 1

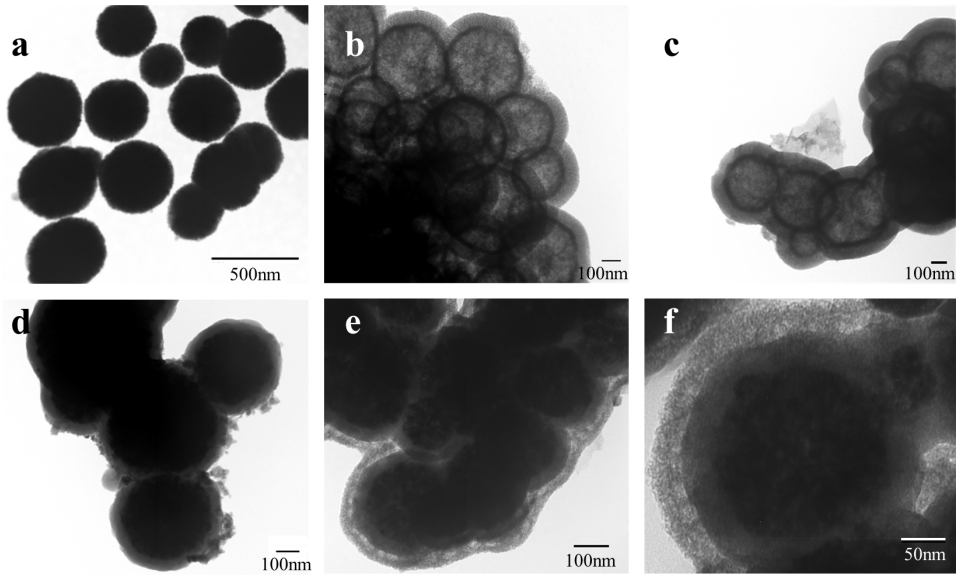

Fig. 2

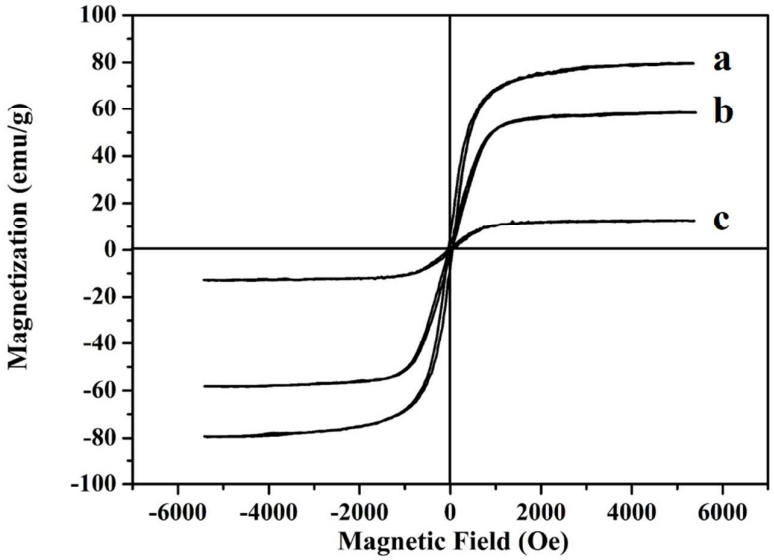

Fig. 3

Fig. 4

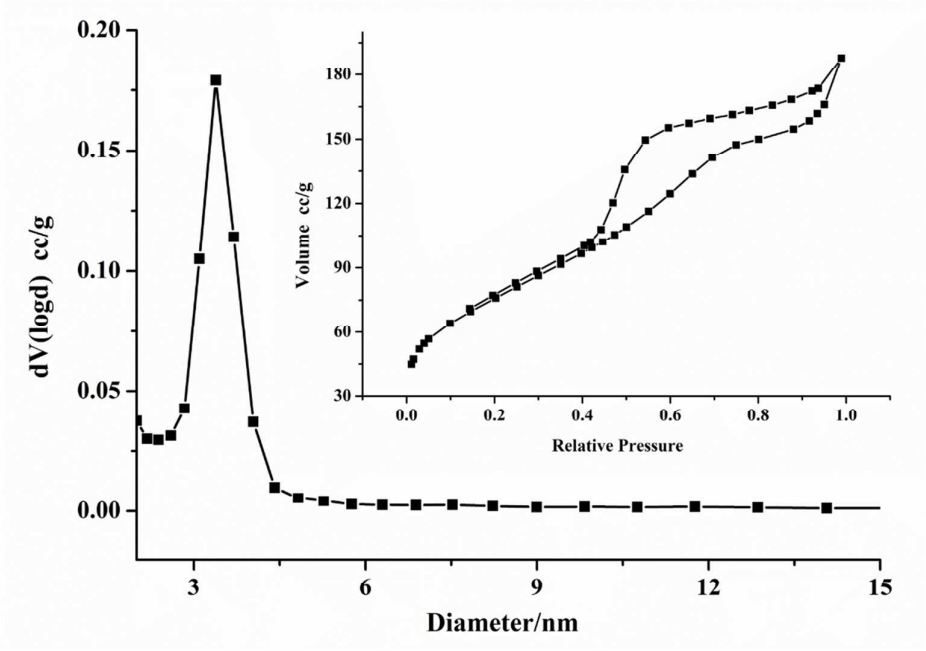

Fig. 5

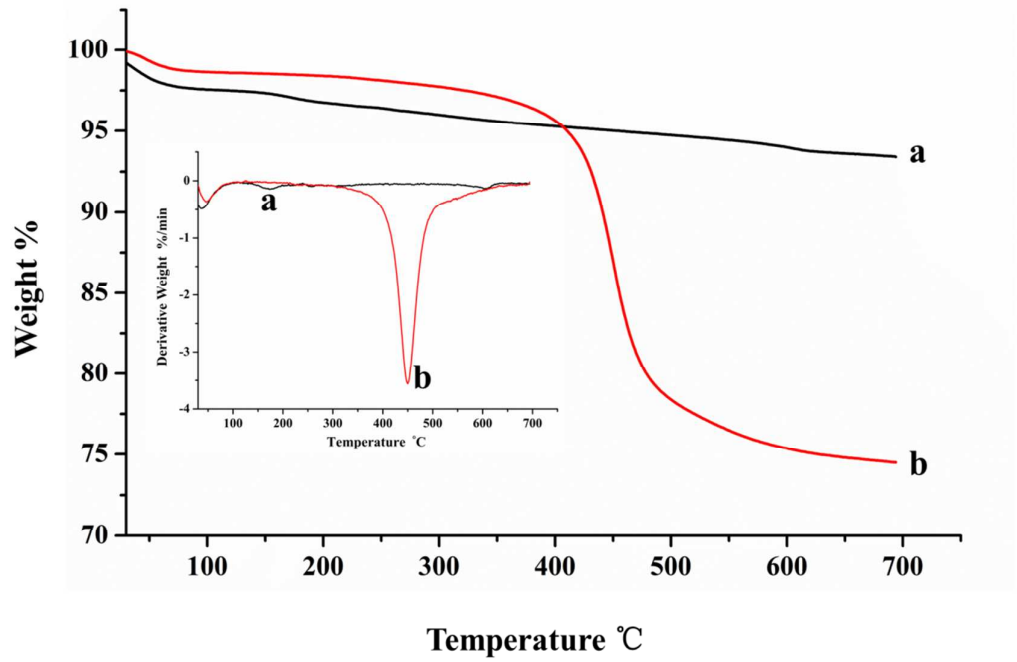

Fig. 6

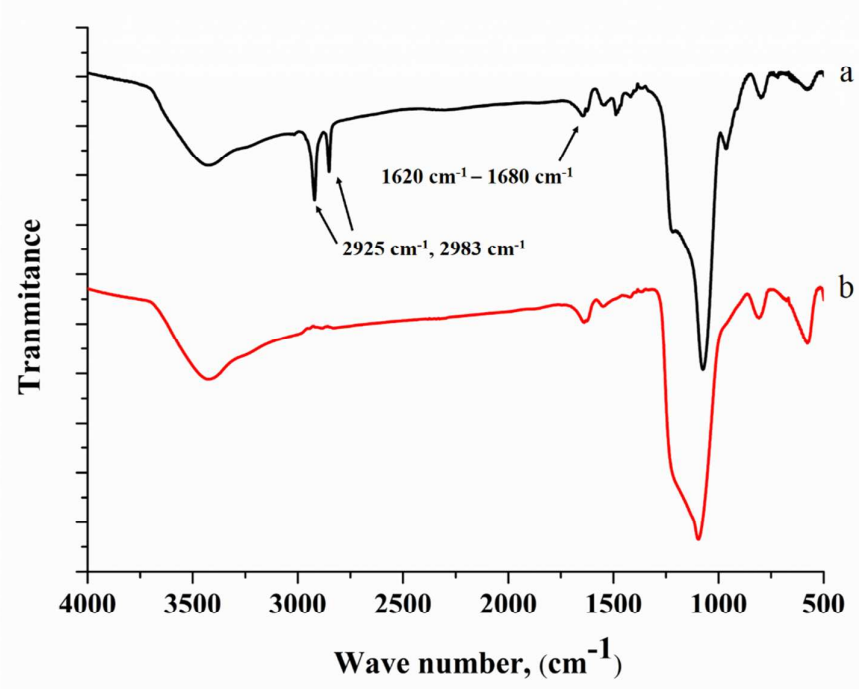

Fig. 7

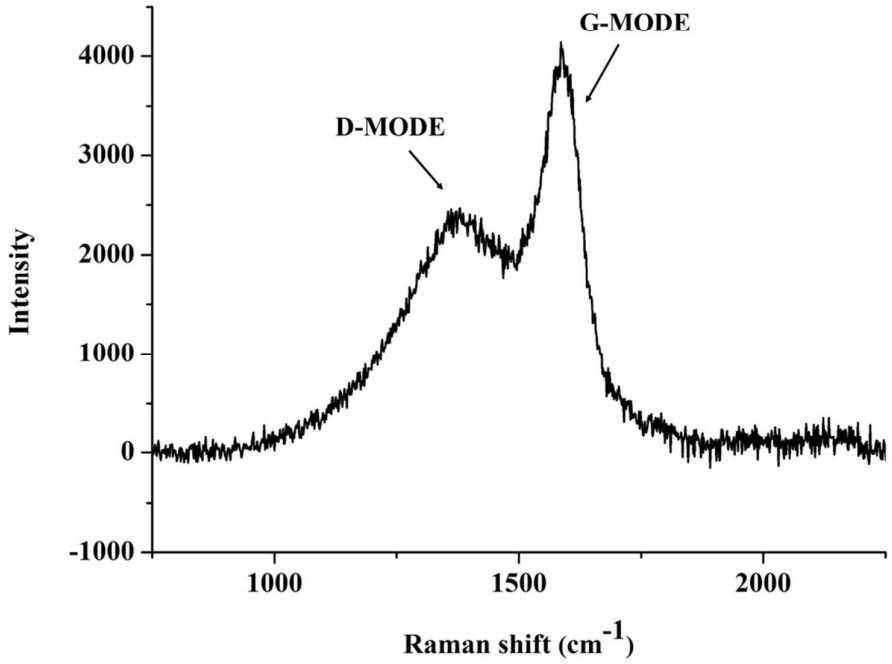

Fig. 8

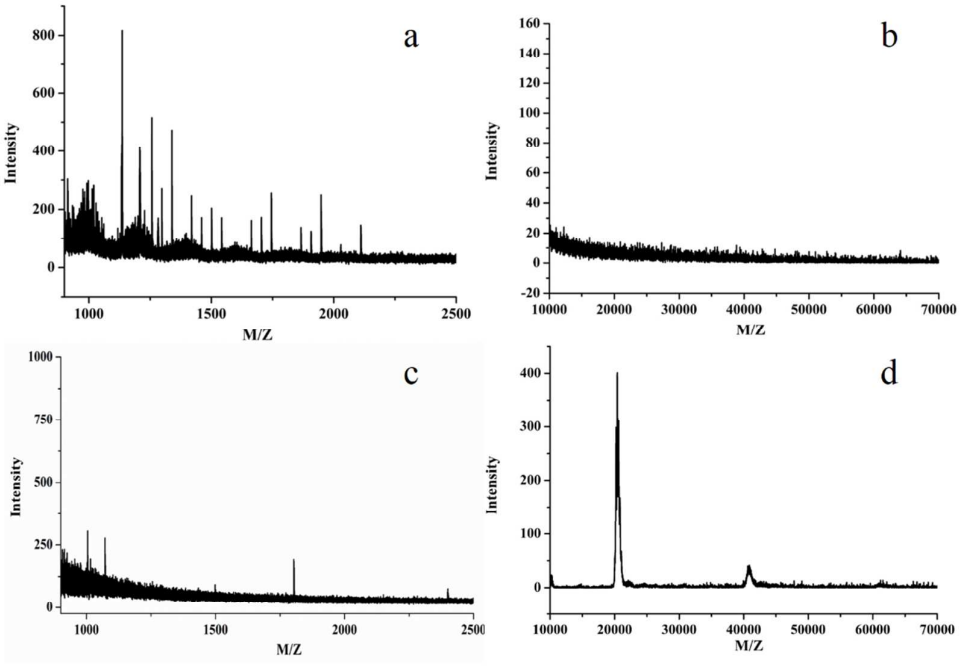

Fig. 9

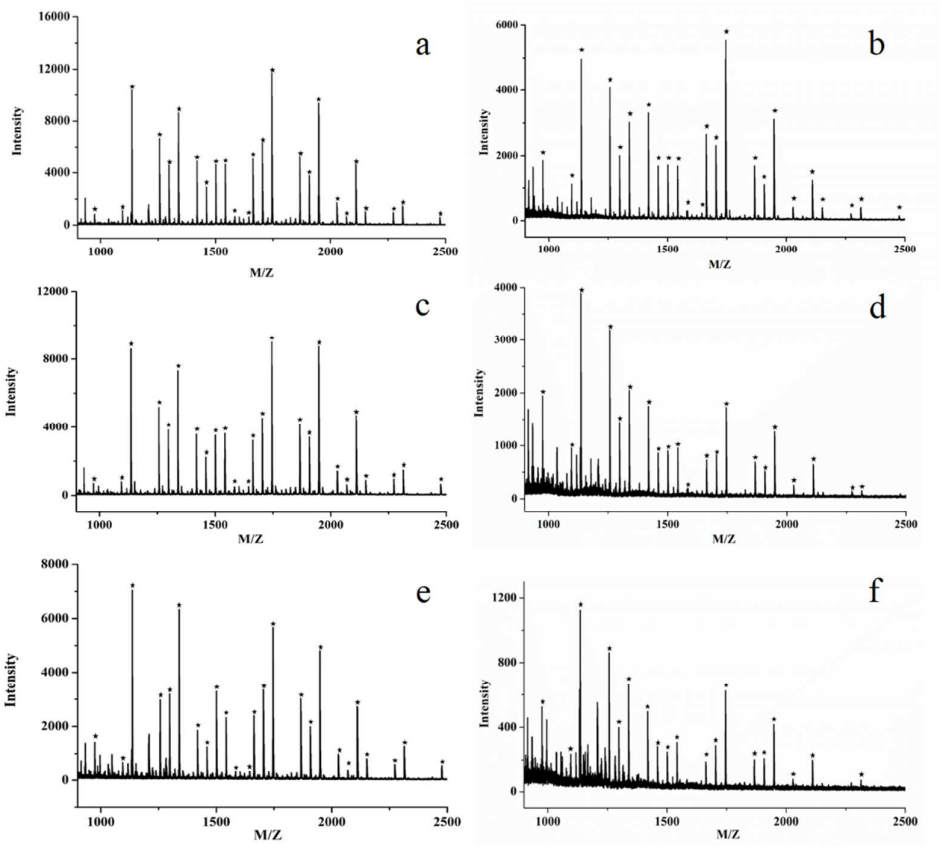

Fig. 10